23rd ABCM International Congress of Mechanical Engineering
December 6-11, 2015, Rio de Janeiro, RJ, Brazil

NUMERICAL COMPARISON BETWEEN TWO DIFFERENT CONSTITUTIVE MODELS FOR SHAPE MEMORY ALLOYS

Marcello Almeida de Paula
Alberto Paiva
Darlene Souza da Silva Almeida
Dionisio Jose Rodrigues da Costa

Universidade Federal Fluminense
Volta Redonda School of Engineering
Department of Mechanical Engineering
420 Trabalhadores Av.
Volta Redonda – RJ – Brazil – 27.255-250
marcellopaula@ig.com.br; paiva.ufrj@gmail.com (corresponding author); darlene.s.s@hotmail.com

Abstract. *The constitutive modeling of the hysteretic behavior inherent to smart materials is a challenging task, no matter which scale is adopted. Concerning Shape Memory Alloys (**SMA**), there is a number of constitutive formulations, which are well-established in the literature and have been widely used by the research community. Nevertheless, each of them has its advantages and drawbacks, depending on the scope of application. Within this context, the main point is to provide the easiest model capable of describing the widest variety of phenomena. This work aims to compare two one-dimensional constitutive theories, highlighting that, despite of their simplicity, both of them are able to describe most of the thermomechanical behaviors exhibited by **SMA** and, thus, constitute suitable choices to simulate **SMA** smart structures applications. The first constitutive theory considers the "assumed transformation kinetics" approach, whereas the second one is based upon internal restrictions. Numerical simulations are performed in order to demonstrate the capability of both models to describe pseudoelastic behavior at different temperatures, shape memory effect and temperature-induced phase transformation, besides their subloops due to incomplete phase transformations, for both tensile and compressive behavior. Along the text, a critical discussion is conducted to elucidate some discrepancies between the two models.*

Keywords: *Shape memory alloy, constitutive model, numerical simulation.*

1. INTRODUCTION

Regarding the constitutive formulation of new intelligent materials, there are plentiful attempts to capture the wide variety of coupled multifaceted phenomena presented by this promising branch. In the specific case of *Shape Memory Alloys* (**SMA**), in the last thirty years, a lot of research effort has been done but there are still some specific behaviors, which remain as a challenge to be modelled. At this point, a paradigm arises: some scientific groups prefer to formulate new constitutive theories to describe these complex phenomena, whereas others try to improve the existing models. Each of these two choices has its own advantages and drawbacks; nevertheless, there are some features that should be observed, no matter which approach is adopted, such as: the number of model parameters to be identified and their physical meanings (model parameters should match real measurable physical/mechanical properties); the mathematical formulation should be friendly to the wide research community; the numerical implementation of the model should be as easy as possible (sometimes, a model is able to capture particular behaviors but its difficulty in implementing may prevent it from obtaining the desired result); the model should be all-inclusive (it is not desirable to have one specific model to represent each phenomenon). More information about **SMA**s' constitutive modeling may be found in reviewing works such as: Birman (1996); Lagoudas (2008), among others.

In the present work, two constitutive theories are compared – namely: the first one concerns the assumed *Phase Transformation Kinetics*' (**PTK**) model proposed by Brinson (1993); the second has to do with the internal restrictions-based approach developed by Savi and co-workers, which has been reported in several references (Savi et al. 2002; Paiva et al. 2005; Oliveira et al. 2010, among others).

2. CONSTITUTIVE MODELS

This section is devoted to present the mathematical equations of the two one-dimensional constitutive models used in this paper. For the sake of simplicity, the equations of both models are presented in their final form, in such a way that the results presented herein can be reproduced at any time, without the need of revisiting the original articles. Nevertheless, for a better comprehension of further details, please check the aforementioned references present in the Introduction section 1.

Concerning the approach proposed by Brinson (1993), the precursor three-dimensional stress-strain-temperature relation, proposed by Tanaka and Nagaki (1982) in a rate format, is reduced to the one-dimensional context, resulting in: $\dot{\sigma} = E\,\dot{\varepsilon} - \alpha\,\dot{\beta} - \Theta\,\dot{T}$
where the state variables are: the axial stress σ ; the axial strain ε ; the internal variable β associated with phase transformation and the absolute temperature T ; whereas the material parameters are: the elastic modulus E ; the scalar parameter α that controls the hysteresis loop height and Θ that is related to the thermal expansion coefficient.

The great contribution introduced by Brinson (1993) lies upon splitting the former scalar internal variable β – originally related exclusively to detwinned martensitic (**M+**) volumetric fraction in Tanaka's work – into two new internal variables, being one of them related to twinned martensite (**M**) named β_T and another one associated with detwinned martensite (**M+**) named β_S, such that: $\beta = \beta_T + \beta_S$.

Brinson performed the analytical integration of the constitutive equation, taking into account the redefined internal variables, where the state variables in the stress-strain-temperature relation denoted by $(\ )_0$ refer to their respective values in the previous time step. Considering the non-diffusive characteristic of the martensitic transformation, the new volumetric fractions β_S and β_T are assumed to depend solely upon the instantaneous values of stress and temperature, resulting in algebraic complementary phase transformation evolution equations that should be rewritten to encompass these new internal variables. Chart 1 summarizes all necessary equations to numerically implement Brinson's model.

Chart 1. Mathematical equations for the constitutive model proposed Brinson (1993).

STRESS–STRAIN–TEMPERATURE CONSTITUTIVE RELATION

$$\sigma - \sigma_0 = E\left(\varepsilon - \varepsilon_0\right) + \alpha\left(\beta_S - \beta_{S_0}\right) - \Theta\left(T - T_0\right)$$

COMPLEMENTARY PHASE TRANSFORMATION EVOLUTION EQUATIONS

DIRECT TRANSFORMATION FOR: $T > M_S$ and $\sigma_S^{CRIT} + C_M\left(T - M_S\right) < \sigma < \sigma_f^{CRIT} + C_M\left(T - M_S\right)$

$$\beta_S = \frac{1-\beta_{S_0}}{2}\cos\left\{\frac{\pi}{\sigma_S^{CRIT} - \sigma_f^{CRIT}}\left[\sigma - \sigma_f^{CRIT} - C_M\left(T - M_S\right)\right]\right\} + \frac{1+\beta_{S_0}}{2} \quad \text{and} \quad \beta_T = \beta_{T_0} - \frac{\beta_{T_0}}{1-\beta_{S_0}}\left(\beta_S - \beta_{S_0}\right)$$

DIRECT TRANSFORMATION FOR: $T \le M_S$ and $\sigma_S^{CRIT} < \sigma < \sigma_f^{CRIT}$

$$\beta_S = \frac{1-\beta_{S_0}}{2}\cos\left[\frac{\pi}{\sigma_S^{CRIT} - \sigma_f^{CRIT}}\left(\sigma - \sigma_f^{CRIT}\right)\right] + \frac{1+\beta_{S_0}}{2} \quad \text{and} \quad \beta_T = \beta_{T_0} - \frac{\beta_{T_0}}{1-\beta_{S_0}}\left(\beta_S - \beta_{S_0}\right) + \Delta_T$$

$$\text{where:} \begin{cases} \Delta_T = \dfrac{1-\beta_0}{2}\left\{\cos\left[A_M\left(T - M_f\right)\right] + 1\right\} & \text{if: } M_f < T < M_S \text{ and } T < T_0 \\ \Delta_T = 0 & \text{else.} \end{cases}$$

REVERSE TRANSFORMATION FOR: $T > A_S$ and $C_A\left(T - A_f\right) < \sigma < C_A\left(T - A_S\right)$

$$\beta_S = \frac{\beta_{S_0}}{2}\left\{\cos\left[A_A\left(T - A_S - \frac{\sigma}{C_A}\right)\right] + 1\right\} \quad \text{and} \quad \beta_T = \frac{\beta_{T_0}}{2}\left\{\cos\left[A_A\left(T - A_S - \frac{\sigma}{C_A}\right)\right] + 1\right\}$$

Regarding the equations provided in Chart 1, some physical quantities should be defined. Firstly, consider the characteristic temperatures of typical **SMA**s, obtained for a free-stress state, namely: the beginning and finishing temperatures for austenite formation, A_s and A_f respectively and the beginning and finishing temperatures for martensite formation, M_s and M_f respectively. Then, for cyclic tests, β_{T0} , β_{S0} and β_0 correspond, respectively, to temperature-induced, stress-induced and total martensitic volumetric fractions' amount prior to the present transformation (remaining from previous transformations), in order to adequately describe the subloops due to incomplete phase transformations. $\sigma_S^{\ CRIT}$ and $\sigma_f^{\ CRIT}$ represent the critical stresses for beginning and finishing direct martensitic phase transformations, respectively. For $T < M_S$, these stress levels remain constant, while the material parameter C_M corresponds to the slope of the linear critical stress increasing for martensitic transformation for $T > M_S$, while C_A is associated to the linear critical stress increasing for reverse transformations. A_M and A_A are material parameters defined as: $A_M = \pi / M_S - M_f$ and $A_A = \pi / A_f - A_S$.

Another assumption adopted by Brinson concers the elastic modulus, which is set as a linear combination of the austenitic elastic modulus (E_A) and the martensitic elastic modulus (E_M), which varies linearly with the total volumetric fraction β, such that: $E(\beta) = E_A + \beta\ (E_M - E_A)$. At last, Brinson conducts an analytical procedure to show that it is possible to relate the model parameter α with the commonly measured material parameter known as maximum residual strain ε_R through the relation: $\alpha = -\varepsilon_R\, E$.

From the numerical point of view, the implementation of Brinson's model is quite simple, since all equations (not only the stress-strain-temperature relation but also the evolution laws) are algebraic. The evolution laws are stress-dependent; therefore, it is simpler to implement the algorithm for prescribed stress, which is aodpted in the present work. It is possible to intoduce the compressive behavior into Brinson's model. In the original model, the stress-induced volumetric fraction varies in the interval [0,1]. Instead of that, it may now vary from [-1,1]; thus, all the limit conditions to apply the evolution laws should be redefined as their modulus. Besides that, in every setep, it is necessary to evaluate the sign of the axial stress σ to verify whether the prescription is a tensile loading or a compressive loading. While conceiving the algorithm, special attention should be devoted for stress-free thermal tests.

Concerning the second model proposed by Savi and co-workers, Paiva et al. (2005) present a one-dimensional simplified version of the updated three-dimensional model presented in Oliveira et al. (2010). In the present work, this easier one-dimensional version is adopted, neglecting classical plasticity and tension-compression asymmetry.

The proposed model considers four internal variables β_1, β_2, β_3 and β_4 representing the respective macroscopic volumetric fractions related to: two variants of detwinned martensite (**M+** associated to tension and **M–** associated to compression); austenite (**A**) and twinned martensite (**M**) induced by temperature. Obviously, it is possible to express one of the internal state variables as a function of the other three. Choosing to eliminate twinned martensite (**M**), i.e.: $\beta_4 = 1 - \beta_1 - \beta_2 - \beta_3$, the following set of constitutive equations arises:

Chart 2. Mathematical equations for Savi's and co-workers constitutive model (Paiva et al. 2005).

STRESS–STRAIN–TEMPERATURE CONSTITUTIVE RELATION

$$\sigma = E\,\varepsilon + \left(\alpha + E\alpha_h\right)(\beta_2 - \beta_1) - \Theta\,\left(T - T_0\right)$$

COMPLEMENTARY PHASE TRANSFORMATION EVOLUTION EQUATIONS

$$\dot{\beta}_1 = \frac{1}{\eta_M}\left\{\alpha\,\varepsilon + \Lambda_M + \left(2\alpha_h\alpha + E\alpha_h^2\right)(\beta_2 - \beta_1) + \alpha_h\left[E\varepsilon - \Theta\left(T - T_0\right)\right] - \partial_{\beta_1} J_\pi\right\} - \partial_{\dot{\beta}_1} J_\chi$$

$$\dot{\beta}_2 = \frac{1}{\eta_M}\left\{-\alpha\,\varepsilon + \Lambda_M - \left(2\alpha_h\alpha + E\alpha_h^2\right)(\beta_2 - \beta_1) - \alpha_h\left[E\varepsilon - \Theta\left(T - T_0\right)\right] - \partial_{\beta_2} J_\pi\right\} - \partial_{\dot{\beta}_2} J_\chi$$

$$\dot{\beta}_3 = \frac{1}{\eta_A}\left\{-\frac{1}{2}(E_A - E_M)\left[\varepsilon + \alpha_h(\beta_2 - \beta_1)\right]^2 + \Lambda_A + (\Theta_A - \Theta_M)(T - T_0)\left[\varepsilon + \alpha_h(\beta_2 - \beta_1)\right] - \partial_{\beta_3} J_\pi\right\} - \partial_{\dot{\beta}_3} J_\chi$$

With respect to the equations presented in Chart 2, the state variables σ, ε and T are the same of Brinson's model, except for the the internal variables $\beta_{(\ )}$, (with: i = 1,2,3) already defined.

Concerning the model parameters, subscripts "*A*" and "*M*" denotes physical/mechanical properties associated to austenite and martensite, respectively, where: $E_{(\ )}$ are the elastic moduli; $\Theta_{(\ )}$ are related to thermal expansion coefficient; $\Lambda_{(\ )}$ are temperature-dependent parameters responsible for beginning critical stress for direct transformations, given by: $\Lambda_M = -L_0^M + \left(L^M / T_M\right)(T - T_M)$ and $\Lambda_A = -L_0^A + \left(L^A / T_M\right)(T - T_M)$; $\eta_{(\ )}$ control the intrinsic **SMA** dissipation and may assume different values for loading $\eta^L_{(\ )}$ and unloading $\eta^U_{(\ )}$ conditions; α_h is a phase transformation parameter that controls the hysteresis loop width and is related to the maximum residual strain ε_R through: $\alpha_h = \varepsilon_R - (\alpha / E_M)$, while the parameters α and T_0 are the same of Brinson's model. Besides, the parameters E and Θ are assumed as linear combinations of their respective austenitic and martensitic values, i.e.:
$E(\beta_3) = E_M - \beta_3(E_M - E_A)$ and $\Theta(\beta_3) = \Theta_M - \beta_3(\Theta_M - \Theta_A)$.

Moreover, $J_\pi(\beta_i)$ is the indicator function with respect to the convex set π that establishes the physical requirement for different phases' coexistence, defined as: $\pi = \left\{ \beta_i \in \Re \,\middle|\, 0 \le \beta_i \le 1;\ \beta_1 + \beta_2 + \beta_3 \le 1 \right\}$ for (i = 1,2,3), whereas $\partial_{\beta_i} J_\pi$ are the subdifferentials of the indicator function J_π with respect to β_i (Rockafeller, 1970). Analogously, $J_\chi(\dot{\beta}_i)$ is the indicator function associated to the convex set χ that provides constraints to enable subloops description.

The numerical implementation of the model proposed by Savi and co-workers need to combine some numerical algorithms well-established in the literature but this is not necessarily complicated. Firstly, notice that the evolution equations of the model are functions of the observable state variables strain and temperature (in Brinson's model, they depend upon stress and temperature); thus, the model is easier implemented for prescribed strain. For prescribed stress – the algorithm here used – it is necessary to adopt an iterative procedure, involving a trial strain state, which should be submitted to a convergence analysis. With respect to the differential evolution equations, they are integrated using the implicit *Euler* method together with the operator split technique, where the internal variables, calculated without considering the subdifferntials, should obey the internal restrictions defined by both convex sets π and χ. If they do not obey, their values should be projected onto each of the two domains (π and χ). For the phases' coexistence constraint, the values of β_i should be orthogonally projected over the nearest surface of the domain defined by the tetrahedron shown in Fig. 2. Besides all that, another iterative procedure should be applied to the set of differential evolution equations, while using the implicit *Euler* method, since the evolution equations are functions of the own internal variables (β_i for: i = 1,2,3), besides the observable state variables.

3. NUMERICAL RESULTS

This section presents a comparison between the numerical results obtained for both models, accompanied by a critical discussion, highlighting some discrepancies between them. Firstly, the models parameters are calibrated through a comparison with pseudoelastic experimental results obtained from the literature. Then, phase transformation due to temperature variation is addressed. After that, isothermal tensile tests considering different temperatures are discussed. Following, a tension-compression isothermal pseudoelastic test is presented. At last, two results for shape memory effect at different initial temperatures are obtained.

Figure (3) presents the comparison between the numerical results obtained by the implemented constitutive model and experimental results obtained by Tobushi *et al*. (1991) for one-dimensional, isothermal, pseudoelastic tests for three different temperatures, aiming the identification of the parameters for both models presented in Tabs. (1) and (2).

Table 1. **SMA** properties and parameters for Brinson's model.

E_A (GPa)	E_M (GPa)	Θ (MPa/K)	ε_R
57	42	0.55	0.0555
M_f (K)	M_s (K)	A_s (K)	A_f (K)
285	295	320	333
C_M (MPa/K)	C_A (MPa/K)	$\sigma_S{}^{CRIT}$ (MPa)	$\sigma_f{}^{CRIT}$ (MPa)
9	8.5	90	170

Table 2. **SMA** properties and parameters for Savi's and co-workers model.

E_A (GPa)	E_M (GPa)	α (MPa)	ε_R
57	42	260	0.0555
L_0^M (MPa)	L^M (MPa)	L_0^A (MPa)	L^A (MPa)
0.15	41.5	0.63	185
η_M^L (MPa/s)	η_M^U (MPa/s)	η_A^L (MPa/s)	η_A^U (MPa/s)
10.35	22	10	22
T_M (K)	T_0 (K)	Θ_A (MPa/K)	Θ_M (MPa/K)
295	280	0.55	0.55

In Fig. 1, the experimental results are monothonic and, thus, exhibit a residual strain after unloading due to the *Transformation Induced Plasticity* (**TRIP**) effect that is out of this work's scope. It is worthwhile to highlight that, after a "training" cyclic process, this effect becomes saturated (resulting in a complete strain recovery) and, therefore, both models are able to capture the correct pseudoelastic behavior. The numerical results for both models are in a good agreement with the experimental results, except for T = 333 K (Fig. 1a); nevertheless, the experimental result does not present a complete phase transformation, which may justify the softening effect at the end of the direct transformation $A \Rightarrow M+$, where the numerical result deviates from the experimental result.

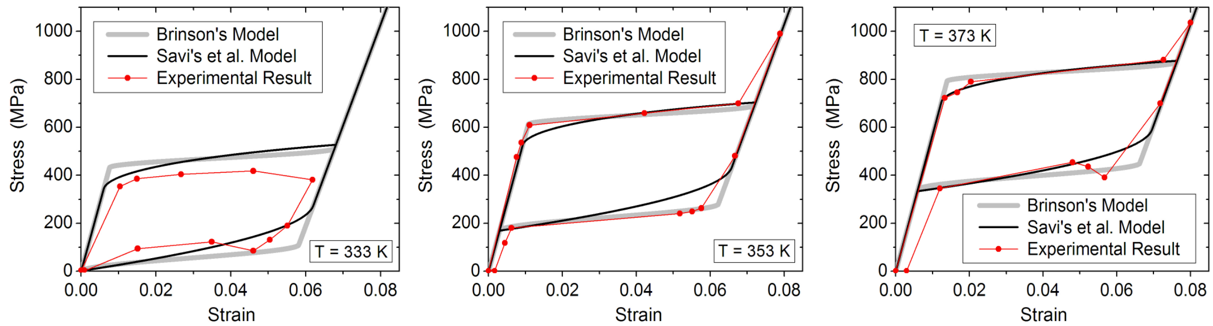

(a) (b) (c)

Figure 1. Comparison between numerical results obtained by both constitutive models and experimental results obtained by Tobushi *et al*. (1991) for different temperature pseudoelastic tensile tests.
(a) $T = 333$K; (b) $T = 353$K; (c) $T = 373$K.

Figure 2 illustrates phase transformation phenomena due to temperature variation for a free-stress state. Figure 2a presents the thermomechanical time prescription; Fig. 2b shows the volumetric fractions' time evolution and Fig. 2c exhibits the temperature-strain diagram.

In Fig. 2a, for a free-stress state ($\sigma = 0$), the thermal loading involves two-and-a-half heating/cooling cycles for both models, being the first cycle such that the maximum/minimum temperature levels overlap the extreme transformation temperatures A_f and M_f, inducing complete phase transformations. The other one cycle and a half have maximum/minimum temperature levels within the transformation temperatures' range, inducing subloops. At this point, an important feature concerning the thermal loading rate should be emphasized. Since Savi's et al. model is rate-dependent and Brinson's not, the same loading rate is adopted for both models and, besides that, proportional loading ends up necessary, in order to preserve the transformation rate in Savi's et al. model. In Brinson's model, these two issues are not mandatory but, for consistency, both of them are assumed as well. Moreover, different loading rates are used during heating and cooling to respect the **SMA** characteristic temperatures. The discrepancy between the two models in the last thermal loading cycle is due to different temperature levels for loading/unloading during subloops for each model.

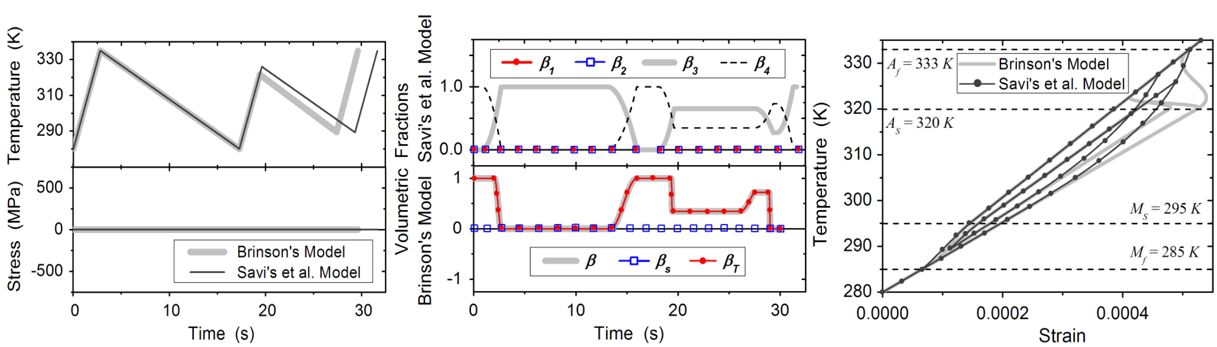

(a) (b) (c)

Figure 2. Free-stress phase transformation due to temperature variation.
(a) Thermomechanical loading; (b) Volumetric fractions' evolution; (c) Stress-strain diagram.

Considering Fig. 2b, initially, at a low temperature (T = 280 K < M_f = 285 K), twinned martensite is the stable phase; thus, for Brinson's model, β_T = 1, while for Savi's et al. model β_4 = 1. While heating the material up to T = 335 K > A_f = 333 K, a complete **M** => **A** reverse transformation takes place and, for Brinson's model, β_T becomes null and for Savi's et al. model, β_4 is substitued for β_3. When the material is cooled back to the low temperature T = 280 K < M_f = 285 K, an **A** => **M** direct martensitic transformation occurs and, as a consequence, for Brinson's model, β_T = 1 again and, for Savi's et al. model, β_4 is substitued for β_3. This first cycle is responsible for the external (envelope) thermal loop. Then, the same process is repeated, without reaching the extreme transformation temperatures A_f and M_f. As a result, intermediate plateaus appear, for $0 < \beta_T < 1$ in Brinson's model and for $0 < \beta_3$, $\beta_4 < 1$ in Savi's et al. model. Eventually, when the material is heated again up to T = 335 K > A_f = 333 K, for Brinson's model, β_T = 0, while, for Savi's et al. model β_3 = 1 and β_4 = 0. In Fig. 2c, it is possible to observe the thermal subloops due to incomplete phase transformations, toghether with the characteristic transformation temperatures: M_f = 285 K, M_s = 295 K, A_s = 320 K and A_f = 333 K, for both models. Notice that Brinson's model is conceived pretty like an algorithm, where, for this test for example, the phase transformation evolution laws should be applied when the limiting temperatures are overlapped. In Savi's et al. model, the phase transformations are intrinsically driven by the own differential evolution equations (together with the internal restrictions for phases' coexistence), without the need of defining limits for beginning and finishing transformations. This characteristic may be viewed as an advantage of Savi's et al. model; however, it is important to observe that the finishing limits in this model are defined by both the loading rate and the dissipation parameter $\eta_{(\ )}$. Again, this feature applies for both temperature-induced transformation and stress-induced transformation, which will be addressed soon in the paper. This counterpoint between the two formulations justifies the discrepancies during subloops description between the two models.

Figure 3 considers the pseudoelastic behavior. Figure 3a presents the thermomechanical time prescription for this test; Fig. 3b shows the volumetric fractions' time evolution and Fig. 3c exhibts the stress-train diagram.

Observing Fig. 3a, there is no temperature variation, while the mechanical loading is composed of a loading/unloading tensile, where the maximum stress level during loading overlaps the critical stress for finishing martensitic transformation, inducing complete transformation. After that, a similar compressive cycle is imposed. Then two subsequent partial loading/unloading tensile mechanical cycles are imposed, inducing subloops. Finally, two analogous compressive partial cycles are performed.

Concerning Fig. 3b, this test is performed at a constant high temperature (T = 373 K > A_f), therefore, for Brinson's model, $\beta_T = 0$ during all the test, while, for Savi's et al. model, $\beta_4 = 0$. At first, the fully austenitic phase is stable; thus, $\beta_S = 0$ for Brinson's model and $\beta_1 = 0$ and $\beta_3 = 1$ for Savi's et al. model. Along with the applied tensile loading, an **A => M+** transformation takes place, i.e.: for Brinson's model $0 < \beta_S < +1$, while for Savi's et al. model β_3 is substitued for β_1. After unloading, the structure returns back to the austenitic phase and, again, $\beta_S = 0$ for Brinson's model and $\beta_1 = 0$ and $\beta_3 = 1$ for Savi's et al. model. When a compressive loading is applied, an **A => M–** transformation occurs and, this time, $0 < \beta_S < -1$ for Brinson's model and β_3 is substitued for β_2 for Savi's et al. model. These loading/unloading processes for tensile and compressive stress induce complete phase transformations that are responsible for the external (envelope) loops in Fig. 3c. Then, according to the stress prescription in Fig. 3a, sucessives partial tensile loading/unloading cycles are imposed, where the maximum/minimum stress levels remains within the beginning and finishing critical stresses range for martensitic/reverse transformations, generating tensile internal subloops in Fig. 3c. For this reason, in Fig 3b, there are, for both models flat plateaus for intermediate values of the internal variables, where, for Brinson's model, $0 < \beta_S < +1$, while, for Savi's et al. model, $0 < \beta_1$, $\beta_3 < +1$, An analogous process is adopted for the compressive behavior.

Figure 3c exhibits the stress-strain diagram, describing both tensile and compressive subloops due to incomplete phase transformations. The dashed red lines crossing the envelope hysteresis loop indicate changes on critical stress values for Savi's et al. model, which is in agreement with experimental verifications (Muller & Xu, 19991), while Brinson's model has fixed values for phase transformations.

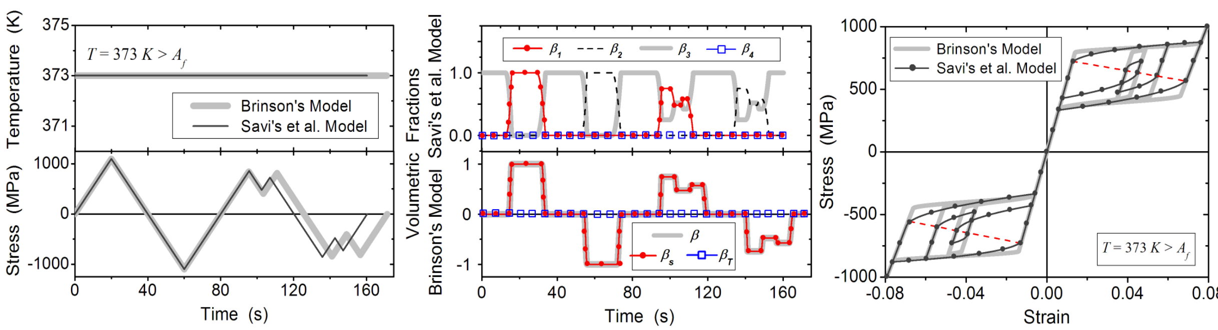

Figure 3. Tension-compression isothermal pseudoelastic test with subloops for T = 373 $K > A_f$.
(a) Thermomechanical loading; (b) Volumetric fractions' evolution; (c) Stress-strain diagram.

Figure 4 illustrates the *Shape Memory Effect* (**SME**) for a partial residual strain situation ($A_S < T < A_f$). Figure 4a shows the thermomechanical time prescription for this test; Fig. 4b shows the volumetric fractions' time evolution and Fig. 4c shows the stress-strain-temperature diagram.

Considering Fig. 5a, for both models, firstly, there are three tensile isothermal mechanical loading/unloading, where, in the first cycle, the maximum stress level during loading overlaps the critical stress for finishing martensitic transformation, inducing complete direct martensitic transformation. The other two are partial loadings, inducing tensile subloops. As follows, a thermal heating/cooling cycle is applied, bringing the sample back to the starting point. Afterwards, the same procedure is applied for compression.

In Fig. 5b, initially, a fully austenitic phase is present with $\beta_S = 0$ for Brinson's model and $\beta_1 = 0$ and $\beta_3 = 1$ for Savi's et al. model. During the first isothermal mechanical tensile loading, a complete **A => M+** transformation takes place, resulting in $\beta_S = +1$ for Brinson's model and β_3 is substitued for β_1 for Savi's et al. model. After the first mechanical tensile unloading, there is still **M+** fraction, due to a partial reverse transformation **M+ => A** and, thus, $0 < \beta_S < +1$ for Brinson's model and $0 < \beta_1$, $\beta_3 < +1$ for Savi's et al. model. Afterwards, subsequent mechanical loading/unloading processes are imposed, such that the intermediate plateaus in Fig. 5b are associated to mechanical subloops. After the complete mechanical tensile unloading, the remaining **M+** fraction vanishes, together with the residual strain, upon heating the material above A_f. In the next step, the material is cooled, bringing the structure back to the original austenite phase with $\beta_S = 0$ for Brinson's model and $\beta_1 = 0$ and $\beta_3 = 1$ for Savi's et al. model. An analogous procedure is developed for compression.

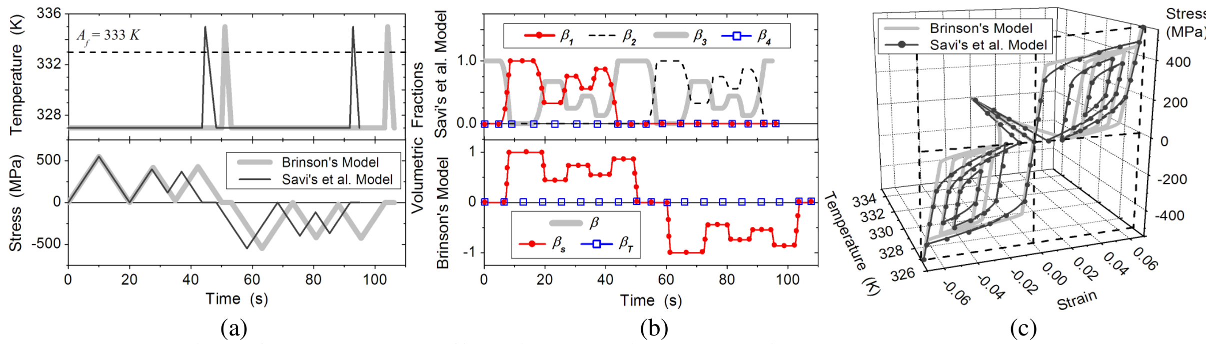

Figure 5. Shape memory effect with mechanical subloops for $A_S < T = 327\ K < A_f$.
(a) Thermomechanical loading; (b) Volumetric fractions' evolution; (c) Stress-strain-temperature diagram.

Figure 5c shows a similar behavior for stress-strain behavior with mechanical subloops compared to those discussed in the previous test (Fig. 4). While performing the subloops, there is a residual strain reduction, such that Savi's et al. model recovers more than Brinson's model. This is due to the fixed limits for phase transformation in Brinson's model. After the complete mechanical tensile unloading, the remaining residual strain is recovered through thermal heating above A_f ($\varepsilon \times T$ plane, in Fig. 5c, for $\sigma = 0$), where the lasting **M+** fraction undergoes a **M+** => **A** transformation. Eventually, the material is cooled back to the initial test's temperature. During cooling, no transformation takes place, since austenite is a stable phase at the former temperature $T = 327\ K > A_S$.

Figure 6 presents the **SME** effect for a low-temperature situation (initial temperature $T = 280\ K < M_f$). Figure 6a shows the thermomechanical time prescription for this test; Fig. 6b exhibits the details of the thermally-induced subloops; Fig. 6c shows the volumetric fractions' time evolution and Fig. 6d shows the stress-strain-temperature diagram.

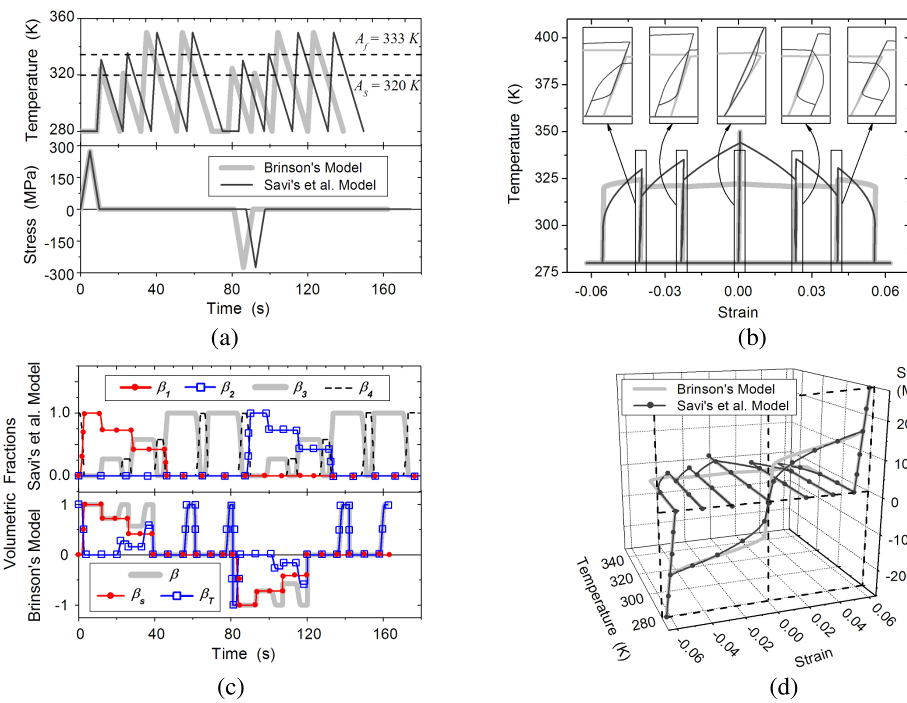

Figure 6. Shape memory effect with thermal subloops for $T = 280\ K < M_f$. (a) Thermomechanical loading;
(b) Details of thermal subloops; (c) Volumetric fractions' evolution; (d) Stress-strain-temperature diagram.

According to Fig. 6a, initially, for both models, a loading/unloading isothermal mechanical tensile cycle is imposed. Then, for a free-stress condition ($\sigma = 0$), two subsequent heating/cooling partial thermal cycles, from $T < M_f$ to $A_S < T < A_f$ and vice-versa, are imposed. After that, two complete thermal cycles, from $T < M_f$ to $T > A_f$, are imposed, returning to its initial twinned martensitic stable state. The same procedure is conducted for compressive behavior.

In Fig. 6c, firstly, twinned martensite is the only stable phase; thus, $\beta_T = 1$ for Brinson's model and $\beta_4 = 1$ for Savi's et al. model. During the first isothermal mechanical tensile loading, a martensitic reorientation process **M => M+** occurs, and, for Brinson's model, β_T is converted into β_S, while, for Savi's et al. model, β_4 is converted into β_1. After mechanical unloading, there is no reverse transformation, remaining $\beta_S = +1$ for Brinson's model and $\beta_1 = 1$ for Savi's et al. model. During the first thermal sub-cycle, while heating such that $A_S < T < A_f$, a partial **M+ => A** transformation takes place. While cooling back to the original temperature (T = 280 K $< M_f$), an **A => M** transformation occurs but only the partial **A** fraction that was previously induced during heating is converted back into **M** fraction. During the second thermal sub-cycle, while heating, both martensitic fractions (M and M+) are converted into austenite. After that, during cooling, the **A => M** transformation is partial again. The intermediate plateaus in Fig. 6c attest the thermal subloops. Next, there is a complete residual strain recovery through heating the material above A_f . Finally, a cooling/heating cycle from $T > A_f$ to $T < M_f$ and vice-versa is imposed to obtain the external thermal "envelope" loop (central detail in Fig. 6b). An extra cooling is necessary to bring the structure back to its initial twinned martensitic stable state, before starting the same procedure for compression.

Figure 6d concerns the stress-strain-temperature diagram, where, during the tensile isothermal mechanical cycle, in the $\sigma \times \varepsilon$ plane, it is possible to identify both the **M => M+** reorientation process and the maximum residual strain (ε_R = 0,0555) after the product phase (**M+**) elastic recovery. Then, for a free-stress state, it is possible to observe thermal subloops, during the residual strain recovery range ($\varepsilon \times T$ plane, for $\sigma = 0$). Subloops' formation mechanism has already been discussed, during the previous explanation for Fig. 6c. These subloops are presented in the two right details depicted in Fig 6b, while the central detail corresponds to the external thermal "envelope" loop. An analogous procedure is adopted for compression, where the two left details depicted in Fig 6b represent the thermal subloops during compressive residual strain recovery. Another complete external thermal "envelope" loop associated with the compressive recovery is superposed to that obtained during tensile residual strain recovery. Despite the fact that both models coherently capture the thermal subloops, which was clarified through the volumetric fractions' evolution in Fig. 6c, according to the details depicted in Fig. 6b, Savi's et al. model present more pronounced subloops, which better agree with experimental results (Miller & Lagoudas, 2000).

4. CONCLUDING REMARKS

This paper deals with the comparison between two constitutive formulations (Brinson's model and Savi's et al. model) based on different approaches. A critical discussion reveals not only differences in their formulations but also discrepancies in the numerical results obtained for three basic thermomechanical behaviors – phase transformation due to temperature variation, pseudoelasticity and shape memory effect, considering subloops. Brinson's model demonstrates to be easier to be implemented, while Savi's et al. model capture more accurately some **SMA** specific features, experimentally observed.

5. ACKNOWLEDGEMENT

The authors would like to acknowledge the support of the Brazilian Research Agencies CNPq, CAPES, FAPERJ as well as INCT-EIE (National Institute of Science and Technology - Smart Structures in Engineering). The acknowledgement applies also to Air Force Office of Scientific Research (AFOSR).

6. REFERENCES

Birman, V.; 1997; "Review of Mechanics of Shape Memory Alloys Structures"; *Applied Mechanics Review*; Vol. 50; N. 11; pp. 629–645.

Brinson, L.C., 1993, "One Dimensional Constitutive Behavior of Shape Memory Alloys: themomechanical derivation with non-constant material functions and redefined martensite internal variable", Journal of Intelligent Material Systems and Structures, Vol. 4, pp. 229–242.

Lagoudas, D.C.; 2008; "Shape Memory Alloys – Modeling and Engineering Applications"; *Ed. Springer*; 435 pp.

Miller, D.A. & Lagoudas, D.C.; 2000; "Thermo-Mechanical Characterization of NiTiCu and NiTi SMA Actuators: Influence of Plastic Strains" *Smart Materials and Structures*; Vol. 5; pp.640–652.

Muller, I. & Xu, H.; 1991; "On the Pseudoelastic Hysteresis"; Acta Metallurgica et Materialia; Vol. 39; N. 3; pp. 263–271.

Oliveira, S.A.; Savi, M.A. & Kalamkarov, A.L.; 2010; "A Three-Dimensional Constitutive Model for Shape Memory Alloys"; *Archive of Applied Mechanics*; Vol. 80; pp. 1163–1175.

Paiva, A. ; Savi, M. A. ; Braga, A. M. B. ; Pacheco, P. M. C. L. . A Constitutive Model for Shape Memory Alloys Considering Tensile-compressive Asymmetry and Plasticity. *International Journal of Solids and Structures*; Vol. 42; N. 11–12; pp. 3439–3457.

Savi, M.A.; Paiva, A. ; Baêta Neves, A.P. & Pacheco, P.M.C.L.; 2002; "Phenomenological Modeling and Numerical Simulation of Shape Memory Alloys: a Thermo-plastic-phase Transformation Coupled Model"; *Journal of Intelligent Material Systems and Structures*; Vol. 13; N. 5; pp. 261–274.

Tanaka, K. & Nagaki, S.; 1982; "Thermomechanical Description of Materials with Internal Variables in the Process of Phase Transformation"; *Ingenieur – Archives*; Vol. 51; pp. 287–299.

7. RESPONSIBILITY NOTICE

The authors are the only responsible for the printed material included in this paper.